LASER INTERFEROMETER GRAVITATIONAL WAVE OBSERVATORY
- LIGO -
CALIFORNIA INSTITUTE OF TECHNOLOGY
MASSACHUSETTS INSTITUTE OF TECHNOLOGY

Technical Note	**LIGO-T1400298–v1**	2014/05/03

Simulation Study for aLIGO Lock Acquisition

Kiwamu Izumi, Sheila Dwyer and Lisa Barsotti
for the aLIGO simulation team

Distribution of this document:

LIGO VIRGO scientific collaboration, and public

California Institute of Technology
LIGO Project, MS 100-36
Pasadena, CA 91125
Phone (626) 395-2129
Fax (626) 304-9834
E-mail: info@ligo.caltech.edu

Massachusetts Institute of Technology
LIGO Project, NW22-295
Cambridge, MA 02139
Phone (617) 253-4824
Fax (617) 253-7014
E-mail: info@ligo.mit.edu

LIGO Hanford Observatory
PO Box 159
Richland, WA 99352
Phone (509) 372-8106
Fax (509) 372-8137
E-mail: info@ligo.caltech.edu

LIGO Livingston Observatory
19100 LIGO Lane
Livingston, LA 70754
Phone (225) 686-3100
Fax (225) 686-7189
E-mail: info@ligo.caltech.edu

http://www.ligo.caltech.edu/

Contents

1 Overview

This document describes the simulation study for the aLIGO lock acquisition scheme and proposes a possible locking sequence as well as plausible combination of length signals. The linear response of the interferometer is analyzed by *Optickle* [1] in frequency domain and its actual behavior and dynamic, nonlinear part are studied by *end 2 end* [2] in time domain with realistic interferometer configuration and noises.

When the previous simulation study was performed by Barsotti [3], the behavior of the arm length stabilization (ALS) system was not included because ALS was still in a design phase. In addition to it, the interferometer parameters were different from the recent nominal values at that time. In this study, we incorporated the latest parameters and models (such as the triple and quadrupole suspensions, optical parameters, ALS noises and so forth) into the simulation in order to ensure the lock acquisition sequence.

2 Definitions

The definition of the length degrees of freedom are explicitly defined in this section to avoid ambiguities.

2.1 The lengths degrees of freedom

Deviation of all the five degrees of freedom can be expressed by

$$\textbf{DARM deviation: } \delta L_{\rm darm} = \frac{\delta L_x - \delta L_y}{2}, \tag{1}$$

$$\textbf{CARM deviation: } \delta L_{\rm carm} = L\frac{\delta\nu}{\nu} + \frac{\delta L_x + \delta L_y}{2}, \tag{2}$$

$$\textbf{PRCL deviation: } \delta L_{\rm prcl} = l_p\frac{\delta\nu}{\nu} + \delta l_p + \frac{\delta l_x + \delta l_y}{2}, \tag{3}$$

$$\textbf{MICH deviation: } \delta L_{\rm mich} = \frac{\delta l_x - \delta l_y}{2}, \tag{4}$$

$$\textbf{SRCL deviation: } \delta L_{\rm srcl} = l_s\frac{\delta\nu}{\nu} + \delta l_s + \frac{\delta l_x + \delta l_y}{2}. \tag{5}$$

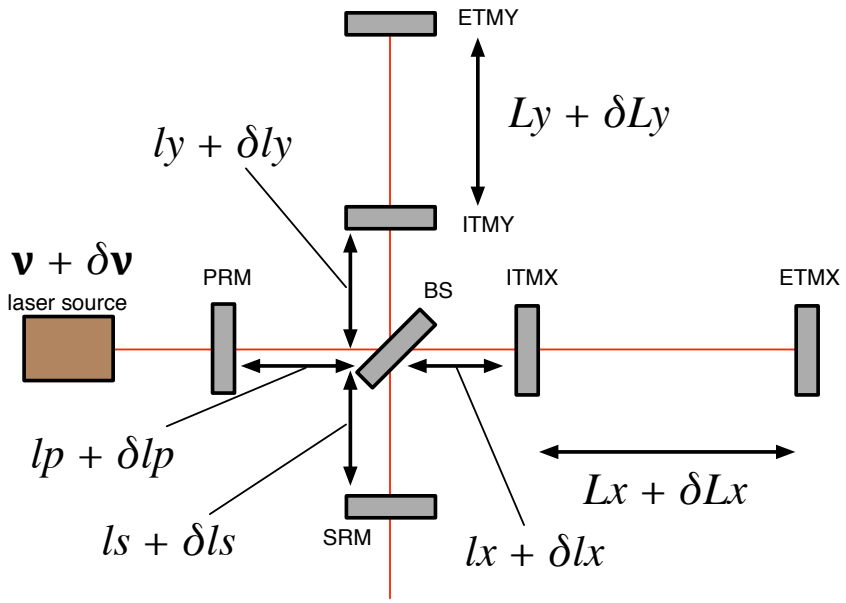

Figure 1: The definitions of the lengths.

For the assignment of the symbols, please refer to figure 1. The quantities with δ in front represent deviations from the nominal values and the nominal values are expressed by symbols without δ. The nominal values are set such the interferometer is locked on the broadband dual-recycled Fabry-Perot interferometer. Note that the averaged arm length L is defined by $L \equiv (L_x + L_y)/2$.

2.2 CARM in frequency

It is often convenient to write CARM in terms of the laser frequency:

$$\textbf{CARM deviation: } \delta\nu_{\rm carm} = \delta\nu + \nu\frac{\delta L_x + \delta L_y}{2L} \tag{6}$$

In fact, an offset in CARM is always expressed in terms of frequency in this document.

3 Interferometer Configuration

3.1 Parameters

A number of important parameters are listed in table 1. They are the same values as the ones used in the aLIGO full lentickle model [4]. We use the high transmissive SRM [5] (i.e. $T = 35\%$ while the final SRM is going to be $T = 20\%$) .

Arm finesse	445
ITM transmissivity	1.4 %
ETM transmissivity	5 ppm
PRM transmissivity	3 %
SRM transmissivity	35 %
Schnupp asymmetry	8 cm
PRC length	57.6562 m
SRC length	50.6654 m
Arm length (both)	3994.5 m
Lower modulation frequency ($f1$)	9,099,471 Hz
Higher modulation frequency ($f2$)	45,497,355 Hz
Modulation depths ($f1$ and $f2$)	0.2

Table 1: Important parameters used in the simulation.

3.2 Signal Recycling

The signal recycling cavity is meant to be locked at the zero-detuning point which is also known as *resonant sideband extraction* or *broadband signal recycling*.

4 The Locking Sequence

4.1 Overview

In order to separate the arm cavities from the DRMI part, we initially bring the arm cavities to a off resonant point by ALS so that neither the carrier nor RF sidebands resonate in the arm cavities. There are various choices for keeping the arm cavities away from resonance – one can have an offset in either DARM, CARM or perhaps combination of these two. In this study, we focus only on a particular case where we put an offset in CARM.

Once the arm cavities are placed at a off resonant point, the DRMI can be now locked by

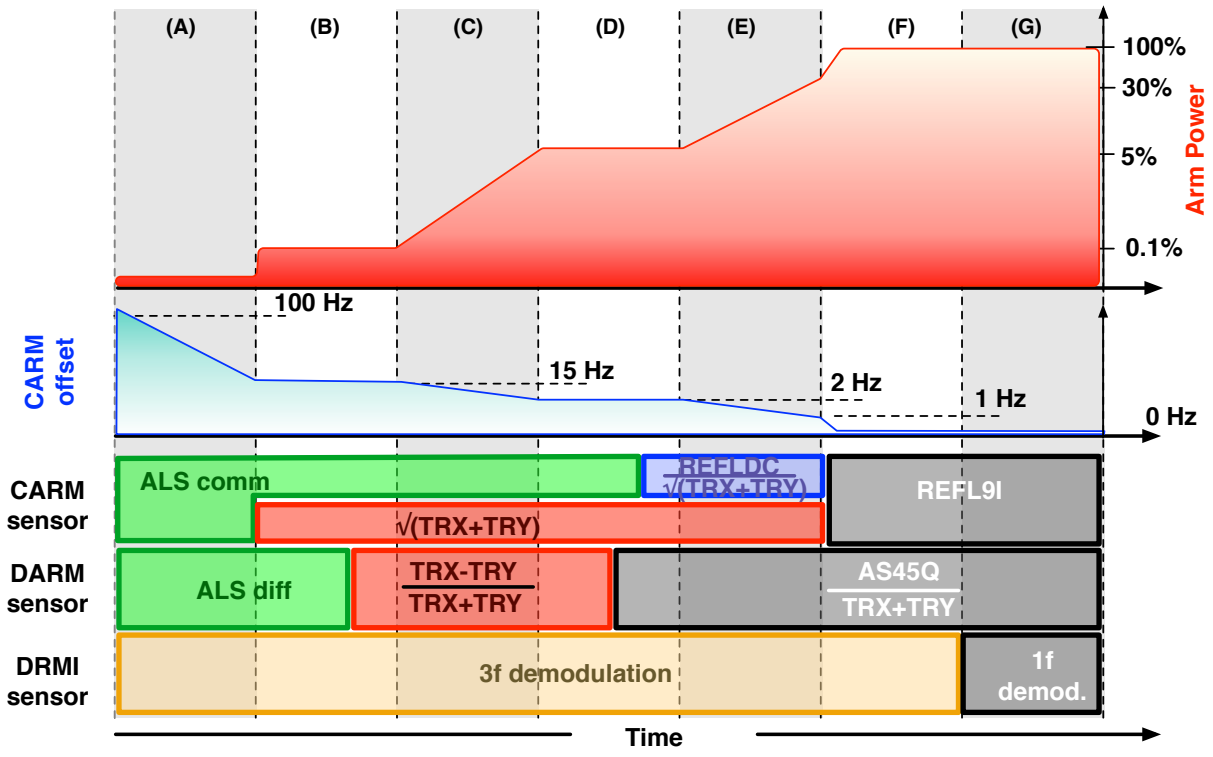

Figure 2: A diagram of the locking sequence.

the signals derived by the third harmonic demodulation technique [6, 3]. We shall call these signals *3f signals* hereafter. As shown in figure 2, we then gradually reduce the CARM offset to zero through multiple steps in each of which the CARM and DARM signals are switched to high-signal-to-noise-ratio signals. Switching the sensors allow to greatly suppress the CARM and DARM fluctuations which are important for minimizing disturbance onto the DRMI.

At some point, the DARM sensor can be completely switched to its final sensor i.e. AS45Q while the CARM is still controlled with temporary sensors. The last important hand-off process is a switch of CARM from temporary signal to the final sensor i.e. REFL9I and this finally gives us the full power build-up in the arm cavities. At this point, one can safely switch the sensors for DRMI to the final ones and this is the end of the locking sequence.

4.2 Steps in detail

4.2.1 Step A: Ground state and initial CARM reduction

At this point, the DRMI is already locked by the 3f signals and CARM has an offset of 100 Hz. Both CARM and DARM are controlled by ALS and hence noisy. The CARM loop feeds the signal back to the laser frequency and DARM to differential ETMX and ETMY. The UGF of CARM should be about 200 Hz in order to avoid injecting sensor noise at high frequencies while maintaining a sufficient suppression at low frequencies [7]. The DARM loop has a UGF of 10-20 Hz in order to suppress the residual DARM motion within 1 nm. The initial CARM offset should be big enough to prevent CARM from an accidental passage through a resonance[1]. Once stable DRMI, CARM and DARM loops are achieved, the CARM offset is reduced to approximately 15 Hz at which the carrier light starts entering the arm cavities.

4.2.2 Step B: CARM low frequency boost and signal handoff in DARM

In this step, the CARM loop is further stabilized at low frequencies by introducing another sensor in addition to ALS comm. For this operation, one can use $\sqrt{\mathrm{TRX} + \mathrm{TRY}}$ (see section 5.2.1) and add it to ALS comm with a cross over frequency of 30 Hz or so. This can be done all in the digital system or through the common mode board. This then stabilizes the power fluctuation of the transmitted light and therefore now one should be able to switch the sensor for DARM from ALS diff to the transmitted light signals.

Before the addition of the squareroot signal, CARM fluctuates by 30 Hz or so due to sensor noise in ALS comm. Therefore the actual CARM may pass through 15 Hz probabilistically during the reduction process performed in step A (section 4.2.1). So for the reason, it maybe perforable to set a trigger for the sum of two transmitted light i.e. TRX +TRY such that it enables a low frequency signal on the CARM loop when TRX+TRY exceeds 0.1% of the full build-up or 50 μW in TRX(Y).

[1] If CARM passes through a resonance with a high speed it produces a Doppler signal which contaminates the SRC signal and breaks the SRC loop due to the saturation in the DACM of SRM.

4.2.3 Step C: CARM offset reduction

The offset is reduced to approximately 2 Hz from 15 Hz. This increases the power build-up to 5% of the maximum or 2.5 mW in TRX(Y). In order to keep the DARM loop stable, one needs to normalize the transmitted signals (see sections 5.1.1 and 5.2.1) or manually adjust the gain when necessary.

4.2.4 Step D: Signal hand off in DARM and CARM

In this stage, one can start using the RF demodulated signal; AS45Q for the DARM control. In principle, AS45Q can introduced in an earlier step, but the optical gain may not be big enough compared to dark noise at high frequencies.

One effect which becomes significant at this point is contamination of the SRCL signal from residual motion in CARM. In order to reduce it, one needs to stop using ALS comm, which is sensor-noise limited, and use REFLDC instead. REFLDC takes care of the high frequency part while the low frequency below 30 Hz is still taken care by $\sqrt{\mathrm{TRX} + \mathrm{TRY}}$ with a careful adjustment of the crossover. In this study, a dynamical normalization (see appendix C) is applied and thus signal is assumed to be digitized. This means that the servo can not be as fast as 300 Hz or so. Therefore the servo UGF stays the same.

4.2.5 Step E: Further CARM offset reduction

The purpose of this step is to reduce the CARM offset down to approximately 1 Hz. This is already within a range where one can obtain a meaningful signal from REFL9I. The power build up at this point is about 30% of the maximum.

4.2.6 Step F: Engagement of REFL9I on CARM

In this stage, one can switch the CARM sensor to the final one i.e. REFL9I. The signal can be directly fedback to the common mode board and therefore the UGF can be high. For instance, 2 kHz is assumed for the UGF in the time domain simulation.

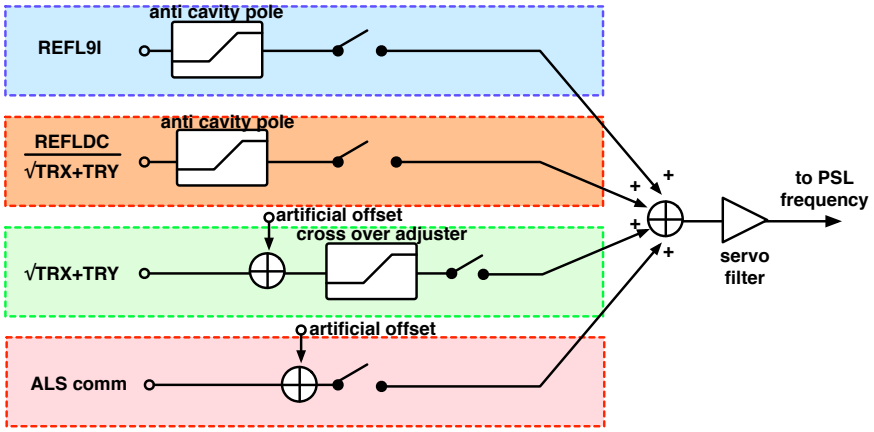

Figure 3: A diagram of common mode signals and their blending.

4.2.7 Step G: Switching the DRMI sensors to the nominal

One should stop using the 3f signals for the DRMI and switch them to the final sensors.

4.3 Time domain simulation

4.3.1 Setup

- Radiation pressure is not included for simplicity.
- The PSL power is set to be 1 W.
- PRM and SRM are modeled as HSTS.
- BS is assumed to be HSTS, which is not true in reality, but for simplicity.
- ETMX and ETMY are modeled as QUAD suspension with a increased drive in UIM by a factor of four as planned [9].
- All the sensors has realistic dark noise. Shot noise is not included for simplicity.
- The simulation clock is set at 13.0 μsec. This should not significantly distort any simulated analog filters[2] up to 3 kHz or so.
- Every optic is continuously excited by simulated seismic noise except ITMs.

[2]IIR filters are used in end 2 end.

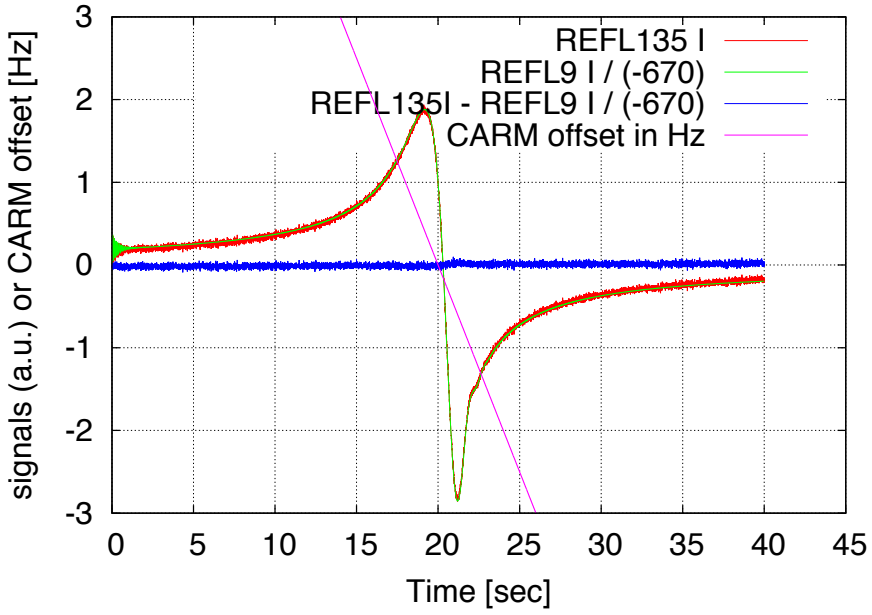

Figure 4: REFL135I and REFL9I signals in time series as CARM sweeps across the resonance. In this simulation run, the rest of degrees of freedom are forced to be at rest at the final operating point.

- ALS diff and ALS comm have realistic sensor noise.
- PSL frequency noise is not included as it should be always suppressed by the CARM loop.
- The IMC control chain is omitted, or in other words, the PSL frequency actuator includes the IMC loop and thus the whole system is dealt as a single input frequency actuator.
- As illustrated in figure 3, the frequency feedback takes four different inputs.

4.3.2 DRMI lock

PRCL is locked using REFL27I with a UGF of 40 Hz and the signal is fedback to PRM. MICH is locked using REFL135Q with a UGF of 20 Hz and the signal is feback to a combination of PRM, SRM and BS to actuate only on MICH. SRCL is locked using REFL135I and REFL9I with a UGF of 20 Hz and the signal is fedback to SRM. The feedback signals applied onto any HSTS is split to the penultimate and bottom stages with a cross over at approximately 3 Hz between them.

In the SRCL 3f error signal, the carrier component mainly due to CARM is subtracted by linearly combining REFL9I in order to avoid a large excursion in SRCL. In figure 4, the simulated REFL135I and REFL9I are plotted to show the effectiveness of the subtraction scheme. This reduces the amount of the excursion from 8-9 nm to 3 nm and improves a saturation issue in the SRM drive.

4.3.3 Simulated sequence

In figure 5, 6 7 and 8, various signals during the simulated locking sequence are shown in time series. Initially, CARM was set to be 50 Hz by introducing an artificial offset in the ALS comm error signal (see figure 3). The DRMI was already locked by the 3f signals as described in section 4.3.2. Both CARM and DARM were controlled by ALS at the begging and sequentially switched to different sensors as described in section 4 as the CARM offset was reduced to zero.

At around $t = 3$ sec, CARM obtained the low frequency boost from $\sqrt{\mathrm{TRX} + \mathrm{TRY}}$ and this improved the stability of CARM at low frequencies as shown in figure 6. The DARM sensor was then switched to TRX-TRY between 4 and 5 sec by linear gain ramping. This introduced slight loop instability in the DARM loop but was not significant. Also DARM became less loud due to better sensor noise in the transmitted light.

After the DARM and CARM loops were stabilized using the transmitted light signals, the CARM offset was then reduced to 2 Hz by changing the amount of the artificial offset that was applied to the square root transmitted light signal (see figure 3).

At around 8 sec, the DARM sensor was switched to AS45Q (section 5.1.2). This also introduced instability during the hand off, but negligible. Next, at around 12 sec, the high frequency part of the CARM loop was handed over to REFLDC from ALS comm. This improved the fluctuation of CARM above 30 Hz as well as the SRCL feedback signal as shown in figure 8. If the sensor was not switch to REFLDC, fluctuations in CARM would saturate the SRM drive in the subsequent steps.

Next, the offset is reduced to 1 Hz and the CARM sensor was switched from the combination of REFLDC and $\sqrt{\mathrm{TRX} + \mathrm{TRY}}$ to the final sensor, namely REFL9 with a much wider control

bandwidth. In the simulation, the gain for REFL9 is set such that the UGF is at 2 kHz when the maximum power buildup is achieved. A glitch occurred in CARM because of the abrupt switching in CARM, but it was much faster than the time scale of CARM, which is about 1 sec, and thus negligible. However, the glitch in the SRCL control can be an issue. According to another simulation run, it is known that the glitch would be much bigger and saturate the SRM drive if REFL9I was not introduced into REFL135I in the SRCL error signal.

As shown in figure 7, SRCL tended to be pulled from the operating point by approximately 3 nm during the sequence even though the carrier component from CARM has been canceled by the subtraction with REFL9I. Therefore this excursion must be due to another coupling, for example from PRCL. This is not crucial from the point of view of a stable SRCL control because the linear range of SRCL is approximately 38 nm and much bigger than the excursion.

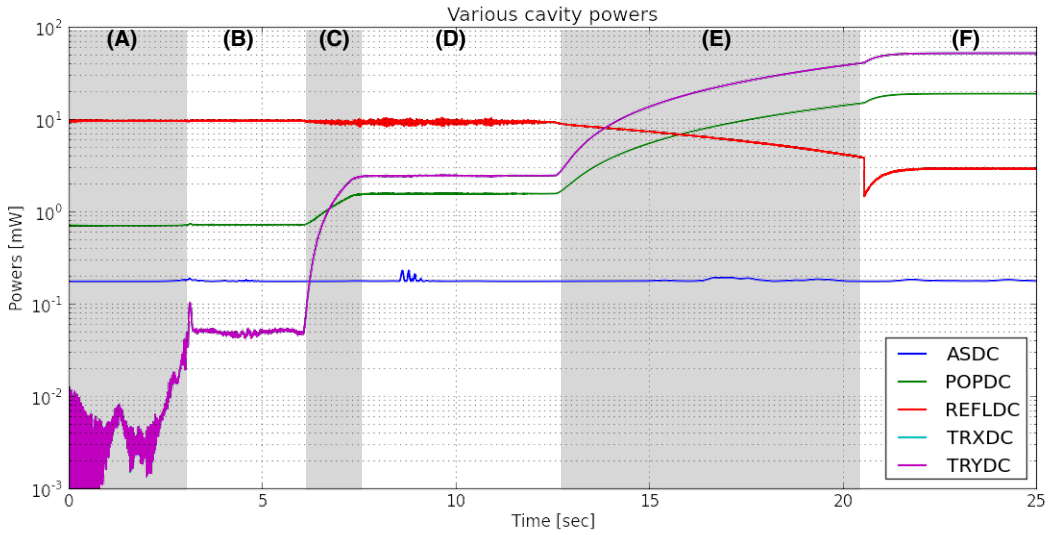

Figure 5: Various cavity powers during the locking sequence in time series.

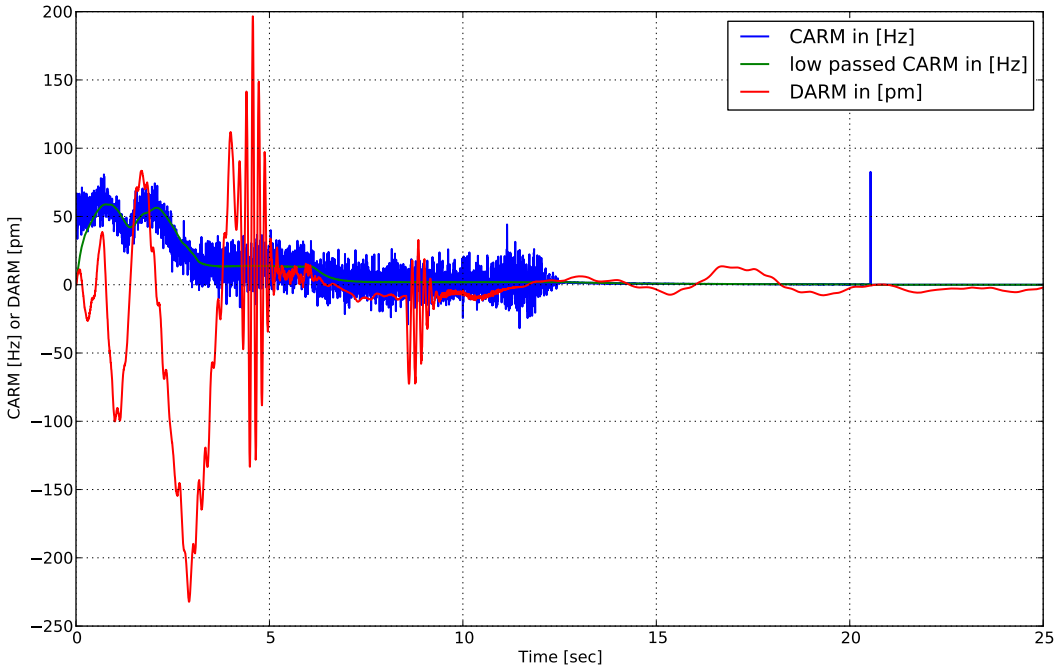

Figure 6: Deviations in DARM and CARM in time series. The low passed CARM uses a single pole low pass with a pole at the cavity pole i.e. 0.8 Hz.

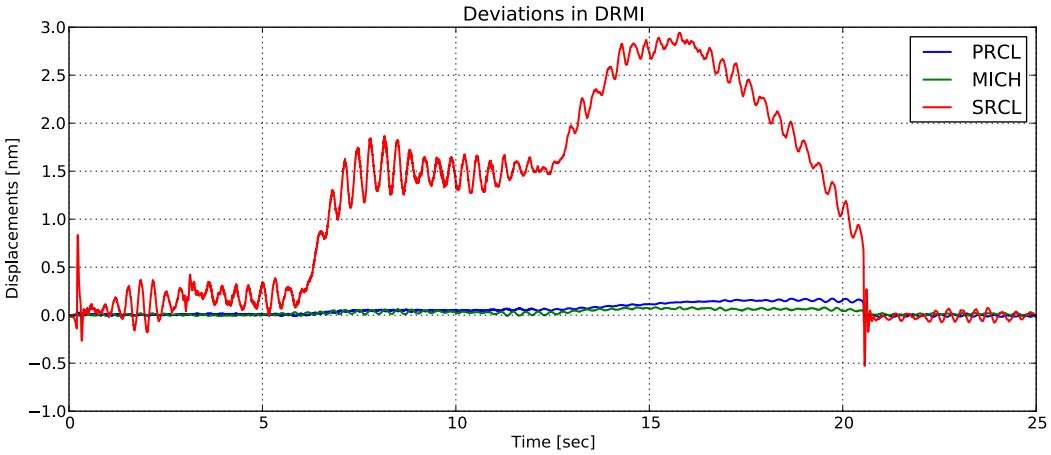

Figure 7: Deviations of DRMI from their operating points in time series.

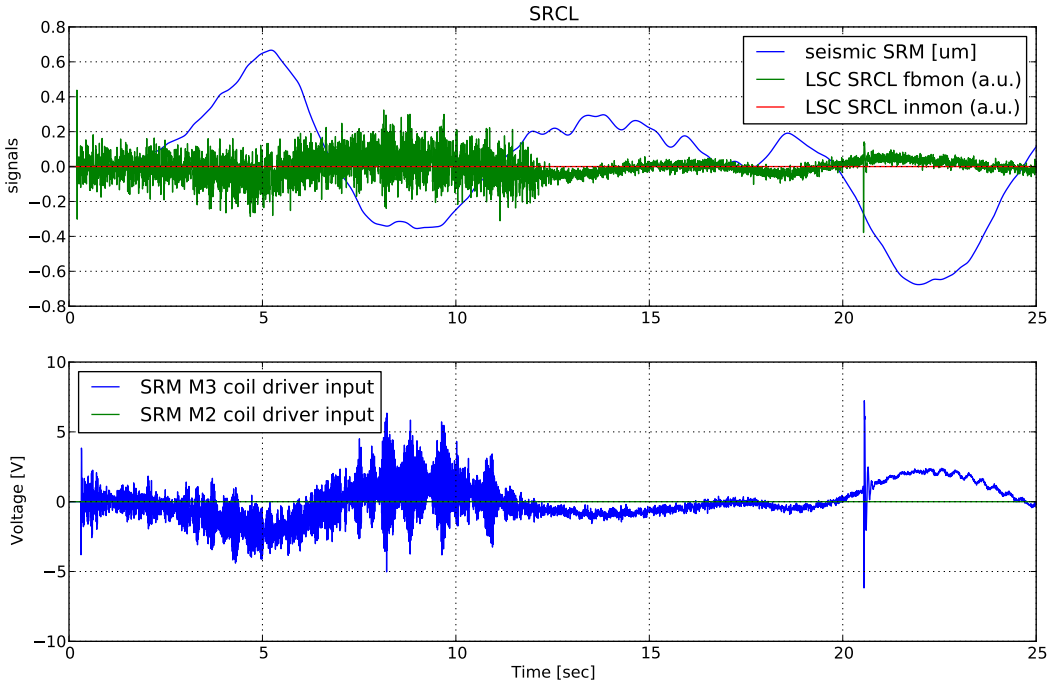

Figure 8: Signals related to the SRCL control in time series.

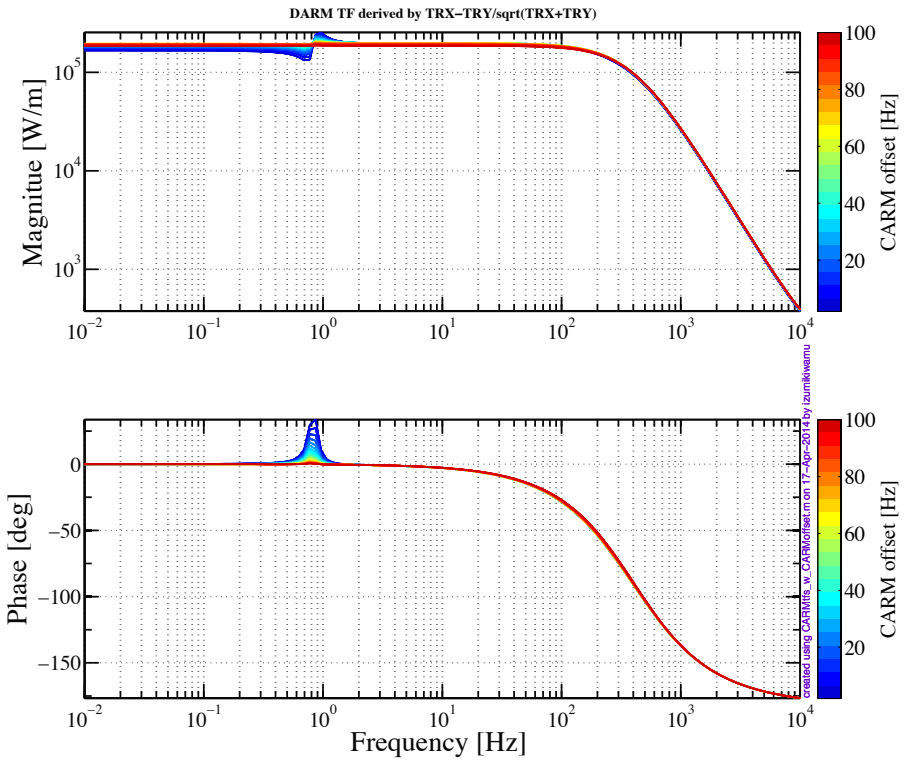

Figure 9: DARM transfer function derived by (TRX − TRY)/(TRX + TRY) at various CARM offset points.

5 Arm cavity signals

Because the DARM and CARM loops utilize various sensors, it is important to analyze each of them as a function of the CARM offset. In this section, we take a close look at how the relevant transfer functions evolve as a function of the CARM offset.

5.1 DARM signals

DARM has two major choices for its sensor as follows:

- DARM $= (\mathrm{TRX} - \mathrm{TRY})/(\mathrm{TRX} + \mathrm{TRY})$
- DARM $= \mathrm{AS45Q}/(\mathrm{TRX} + \mathrm{TRY})$

Also, ASDC is another possible candidate, but it requires to introduce an offset in DARM as well. Because this may complicate the DARM control due to radiation pressure effects, we omit it from the list.

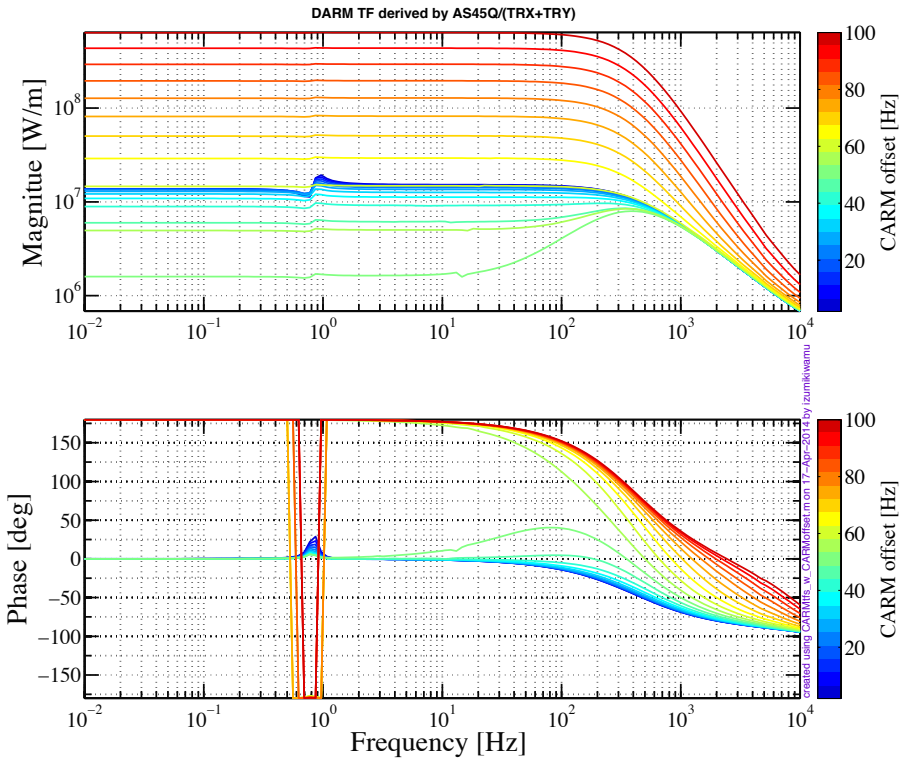

Figure 10: DARM transfer function derived by AS45Q/(TRX + TRY) at various CARM offset points.

5.1.1 (TRX − TRY)/(TRX + TRY)

This is a signal that has been used at the 40-meter lab [8] and studied by Barsotti [3]. Because DARM does not have an offset, the transfer function is flat and clean up to 100 Hz as shown in figure 9. Normally a single arm cavity exhibits its cavity pole at 42 Hz, but it is now pushed to 200 Hz by the signal recycling. Such a relatively high cavity pole makes the design of the DARM loop easier since the loop typically has a low bandwidth at order of 10 Hz. One important point is that its gain grows as CARM approaches to the resonance. Therefore one must compensate the gain change in a dynamical way. So for the reason, the signal is normalized by (TRX + TRY).

One thing which is unclear at the moment is that – in the time domain simulation, this signal needed to be normalized by $(\mathrm{TRX} + \mathrm{TRY})^{1/2}$ for keep the same gain. Additionally, when the SRCL signal did not have the carrier subtraction, the normalization worked well with $(\mathrm{TRX} + \mathrm{TRY})^{3/2}$. Therefore this must be due to an offset in SRCL which then changes the response of DARM. This has not been studied any further as it can be alternatively handled

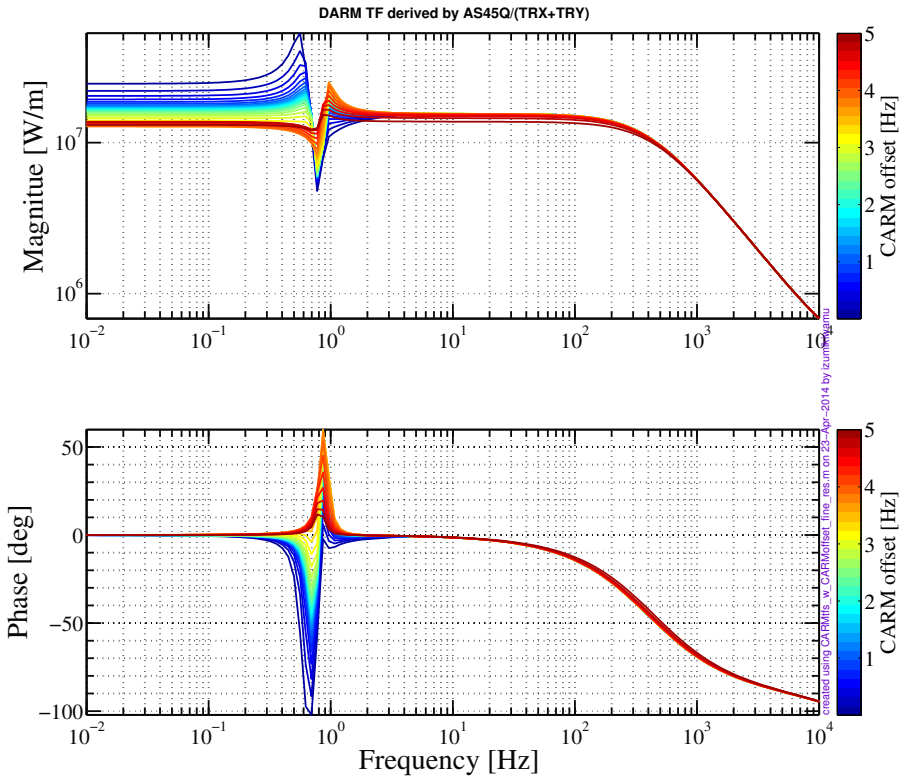

Figure 11: DARM transfer function derived by AS45Q/(TRX + TRY) at various CARM offset points. This is the same plot as figure. 10 but with a different CARM offset range (i.e. 0 - 2 Hz).

by a manual gain adjustment.

5.1.2 AS45Q/(TRX + TRY)

As shown in figure.10, when the CARM is far from the resonance, the sign of AS45Q is opposite. As the CARM gets closer to the resonance, the phase of the carrier light reflected off of the arm cavities flips and the signal starts to be meaningful. This sign transition occurs when the CARM offset is approximately 40 Hz or less. Since this is the final sensor and has a high signal-to-noise ratio, it is good to use this signal when available with a good signal-to-noise ratio. One consideration is the power normalization. Because the arm power increases by a factor of more than 10 from an offset of 2 to 0 Hz. It is necessary to dynamically compensate the optical gain by using the arm cavity power; TRX and TRY. Once the signal is normalized by the sum of TRX and TRY, the optical gain does not change as long as the CARM offset is within ~ 4 Hz as shown in figure 11.

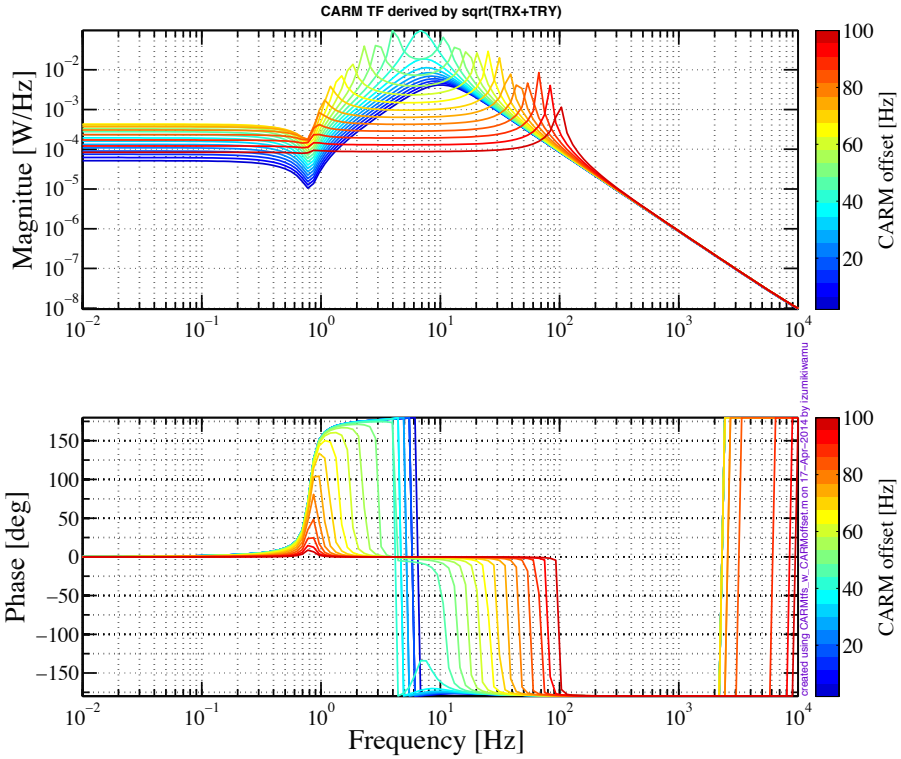

Figure 12: CARM transfer function derived by $\sqrt{\mathrm{TRX} + \mathrm{TRY}}$ at various CARM offset points.

5.2 CARM signals

CARM also has a few choices. However, as opposed to the DARM transfer functions, they show a detuning peak and radiation pressure effects because the CARM is the one which has an offset.

The choices of good signals are listed below:

- CARM = $\sqrt{\mathrm{TRX} + \mathrm{TRY}}$
- CARM = REFLDC
- CARM = REFL9I

Additionally it is possible to use the power recycling cavity power; POPDC. However this signal contains not only the carrier but also the RF sidebands and therefore not preferable when the power-buildup is low.

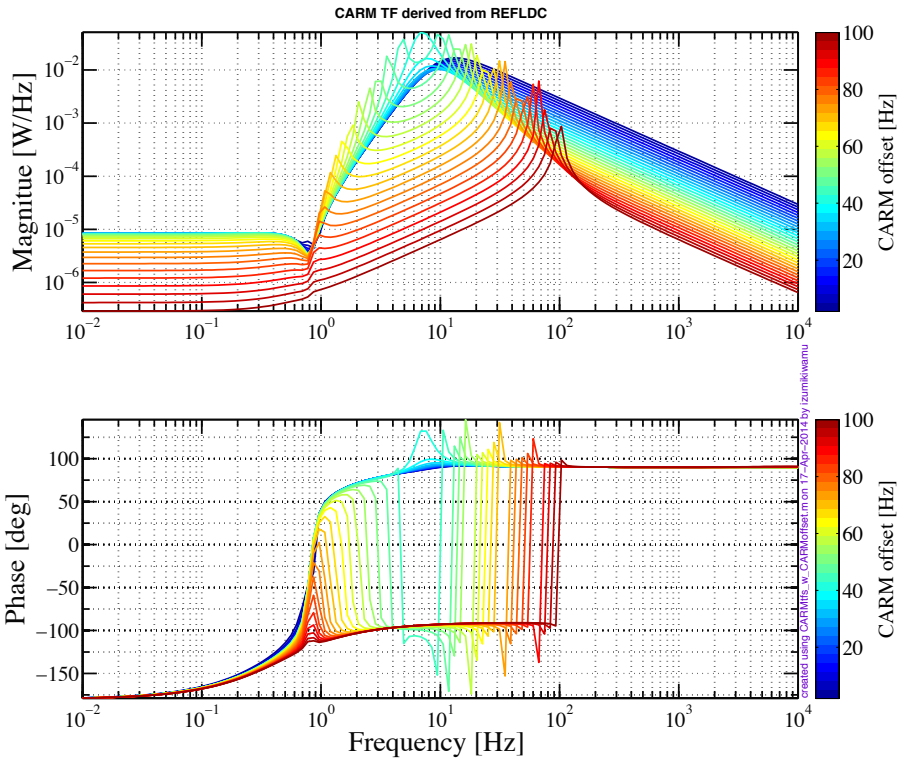

Figure 13: CARM transfer function derived by REFLDC at various CARM offset points.

5.2.1 $\sqrt{\text{TRX} + \text{TRY}}$

This is another signals that has been used and studied [3][8]. An advantage of this signal is that the high frequency feature does not vary regardless of how big the CARM offset is. On the other hand, the low frequency feature (i.e. detuning peak and radiation pressure effect) evolves prominently. As shown in figure.12, the transfer functions of the signal falls off as $1/f^2$.

A noteworthy point is that this signal can not be used for a high-bandwidth control because it is slow — TRX and TRY are digitized by an ADC at the end stations and sent over to the conner station through the digital system.

5.2.2 REFLDC

Another choice is REFLDC. In general, this signal has a big advantage over TRX and TRY – this signal does not have to be digitized and therefore can be fast. As shown in figure. 13, the response is small at low frequencies. On the other hand, the response at high frequency

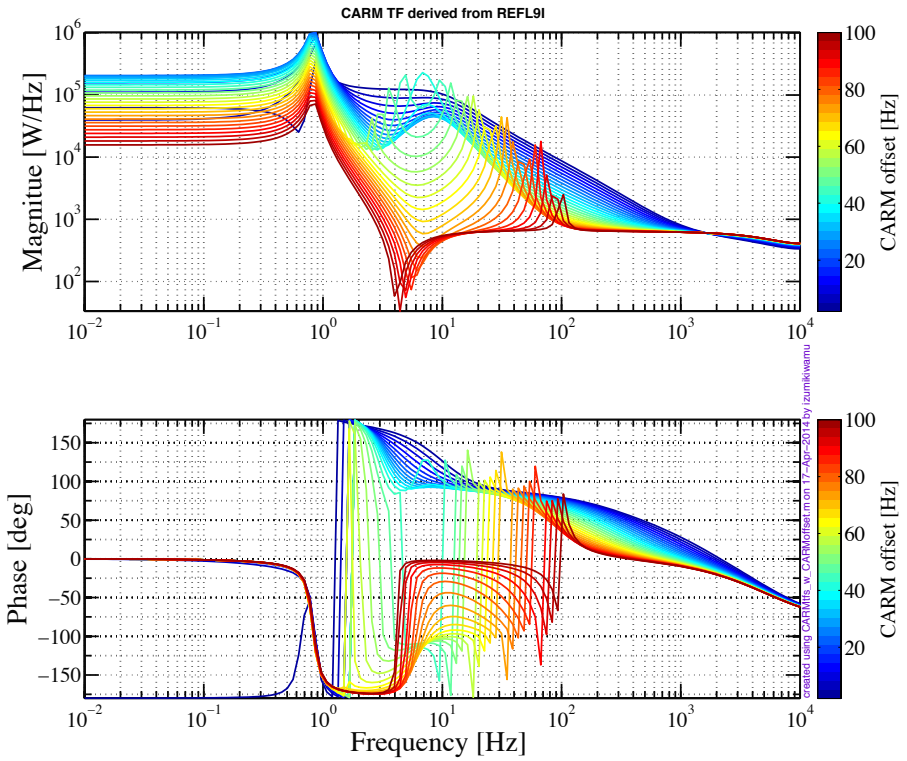

Figure 14: CARM transfer function derived by REFL9I at various CARM offset points.

is clean and falls as $1/f$. This signal is useful if one desires to suppress noises in CARM at high frequencies above the detuning peak.

5.2.3 REFL9I

This is the last signal one can obtain over the course of the offset reduction because of the narrow linear range. As it is shown in figure.14, the transfer function is not straightforward in a frequency range from 1 to 100 Hz. It is reasonable not to use this signal until the CARM is within a couple of Hz.

6 Cross couplings

6.1 CARM and DARM to DRMI

As the CARM approaches to the resonance, the residual motion in CARM and DARM tend to contaminate the 3f signals. In this section, we analyze the effect from CARM and DARM

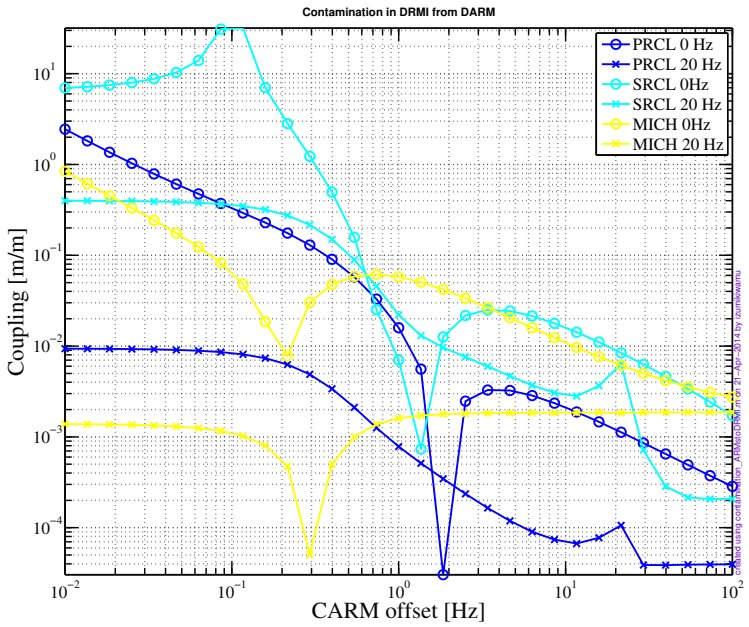

Figure 15: Coupling from DARM into DRMI as the CARM offset changes.

onto the three short DOFs –namely PRCL, MICH and SRCL. In particular, SRCL is mostly disturbed essentially because the SRC has the lowest finesse (~ 14) and hence lowest optical gain. In order to assess the degree of the contamination, a frequency domain study was performed and the results are shown in figure 15 and figure 16.

When CARM offset is at 0.01 Hz, which is essentially equivalent to be on the resonance, the coupling coefficient from DARM to SRCL is approximately 10 meter/meters as shown in figure 15. Even so, this should not be stringent because (A) DARM is already well suppressed in order for DARM to be stably controlled and (B) the intrinsic fluctuation is small in the first lace above a few Hz due to the isolation by QUADs. In fact, no significant disturbance was observed in the time domain study.

On the other hand, the contamination from CARM is much more serious. Because CARM typically has a relatively high control bandwidth, fluctuation above 10 Hz is usually limited by sensor noise. This is different from DARM whose servo does not inject sensor noise above 10-20 Hz. So for the reason, CARM tends to disturb DRMI more than DARM does at high frequencies. In fact, this is exactly the reason why REFLDC needed to be introduced in the locking sequence in order to reduce the noise at high frequencies. This is a serious issue as it can saturate the SRM drive and therefore can unlock the SRCL control. The contamination

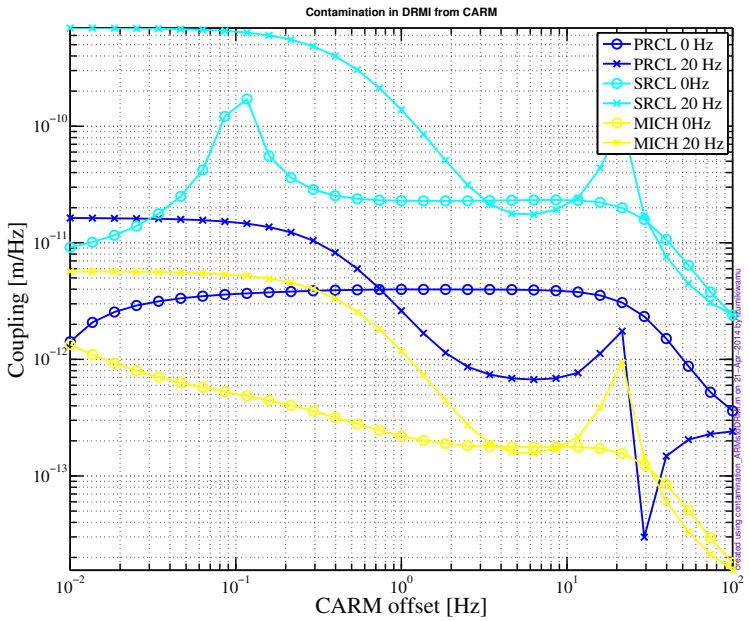

Figure 16: Coupling from CARM into DRMI as the CARM offset changes.

becomes significant as CARM gets closer to the resonance as shown in figure 16.

6.2 Coupling in transmitted light between DARM and CARM

In this subsection, we study a cross coupling between CARM and DARM when the transmitted light are used for their sensors. In such a case, the sensing matrix can be expressed by

$$\begin{pmatrix} \sqrt{\mathrm{TRX}+\mathrm{TRY}} \\ \mathrm{TRX}\ -\mathrm{TRY} \end{pmatrix} = \begin{pmatrix} 1 & \epsilon \\ \eta & 1 \end{pmatrix} \begin{pmatrix} \delta L_{\mathrm{CARM}} \\ \delta L_{\mathrm{DARM}} \end{pmatrix}, \tag{7}$$

where we have normalized the matrix such that the diagonal elements have 1. ϵ and η are the cross coupling terms which should be ideally zero. However, they can be nonzero values if there is a calibration error in the signals and/or difference in losses between two arms.

To evaluate the amount of the cross coupling terms, we introduce an intentional calibration imbalance such that

$$\mathrm{TRY} \rightarrow \mathrm{TRY} \times (1 - \mathrm{imbalance}), \tag{8}$$

where the imbalance takes a value between 0 and 1.

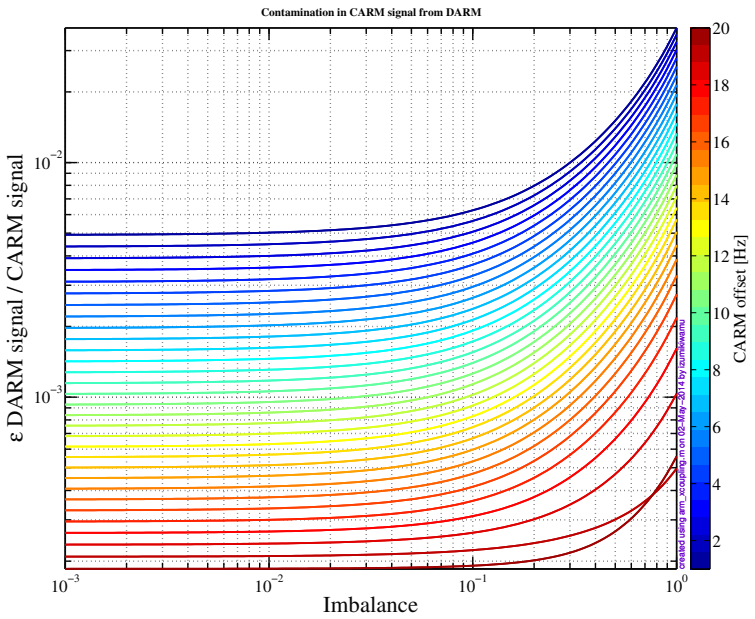

Figure 17: Coupling from DARM into CARM when $\sqrt{\mathrm{TRX} + \mathrm{TRY}}$ is used.

In figure 18 and 17, calculated off-diagonal elements at 20 Hz are shown as a function of the imbalance with the X arm having a bigger loss by 20 ppm that than of the Y arm. This is meant for simulating a realistic situation. Different colors shown in the plots represent various CARM offset points from 20 to 1 Hz.

As shown in figure 17, the contribution from DARM into $\sqrt{\mathrm{TRX} + \mathrm{TRY}}$ is smaller than 1 which is good. As the imbalance increases, the cross coupling increases as well. Also, the cross coupling becomes bigger as CARM approaches to the resonance. If one desires to keep the cross coupling less than 1%, the calibration must be as accurate as 10% which practically should not be difficult.

On the other hand, the coupling from CARM into TRX-TRY is severe. For instance, when the imbalance is at 1%, the contribution from CARM is already as big as 1 with an CARM offset of approximately 14 Hz. Although the CARM residual motion should be well-suppressed by a relatively high bandwidth control (∼200 Hz), this is a worrisome amount. Therefore, in order to have a good decoupling from CARM, one needs to pay an extra attention to the calibration imbalance. Also it is worthwhile to note that the cross coupling improves as CARM approaches the resonance as opposed to $\sqrt{\mathrm{TRX} + \mathrm{TRY}}$.

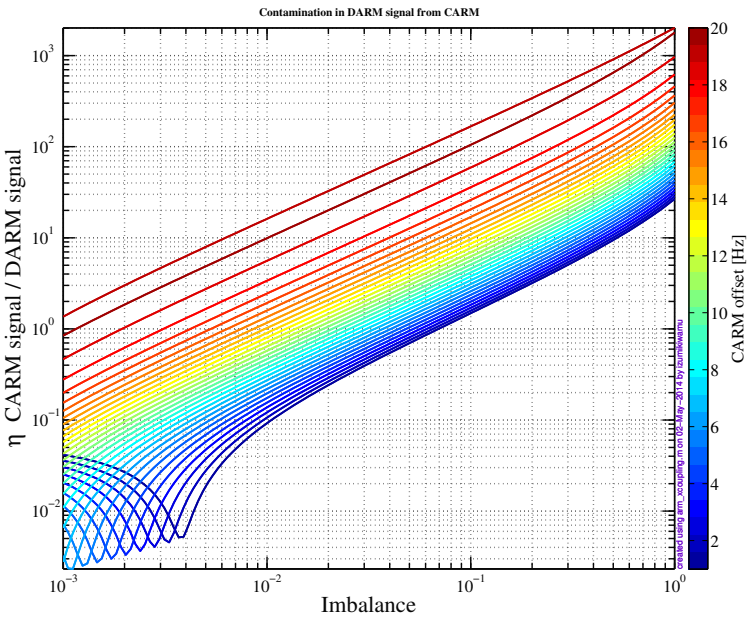

Figure 18: Coupling from DARM into DRMI as the CARM offset changes.

7 Conclusion

We revisited the previous lock acquisition study with the latest models such as noises , actuators and suspensions in the latest interferometer configuration. We conclude that the lock acquisition process can be achieved by employing the third harmonic demodulation scheme for the dual-recycled Michelson part, and combinations of the cavity power signals and the arm length stabilization signals for the arm cavities. This study should aid in better understanding of the dynamical length sensing and control which is the key for lock acquisition.

A Control filters and some parameters

element	zeros (Hz)	poles (Hz)	gain
PSL frequency actuator	-	-	1
anti cavity pole (REFL9I and REFLDC)	1	10k, 30k	1
cross over adjuster for $\sqrt{\mathrm{TRX}+\mathrm{TRY}}$	15, 15	1, 450, 700	80k
CARM servo filter	1, 50	1m, 1m, 1m, 1k	1 at 200 Hz
DARM servo filter	3, 5, 10	0.1, 30, 60, 200	30
DARM boost filter	3.3	1	33
PRCL servo filter	10	100, 500	0.013
MICH servo filter	10	100, 500	0.25
SRCL	10	100, 500	0.56
PRCL, MICH and SRCL boost filters	3	0.1	30
QUAD suspension	-	-	[10]
HSTS suspension	-	-	[11]
REFL attenuator	-	-	40 dB
AS attenuator	-	-	40 dB
TRX and TRY attenuators	-	-	N/A

Table 2: Zeros, poles and gains used in the time domain simulation.

B Maximum offset range

There is a certain limit for the maximum allowed offset in the arm cavity. If the offset is too large in either or both of the arm cavities, one (or both) resonates with the $2 \times f1$ sideband. This occurs when an offset is at about 14 nm in a single arm or equivalently $\sim$ 1 kHz in CARM. A plot of the RF resonances is shown in figure.19.

C Normalization of REFLDC

If one handles REFLDC in the digital system, a normalization can be achieved like the other cavity power signals. In this case, REFLDC exhibits steady, unchanged response at high frequencies when normalized by square root of TRX and TRY. The transfer functions of the normalized signals at various CARM offsets are shown in figure 20.

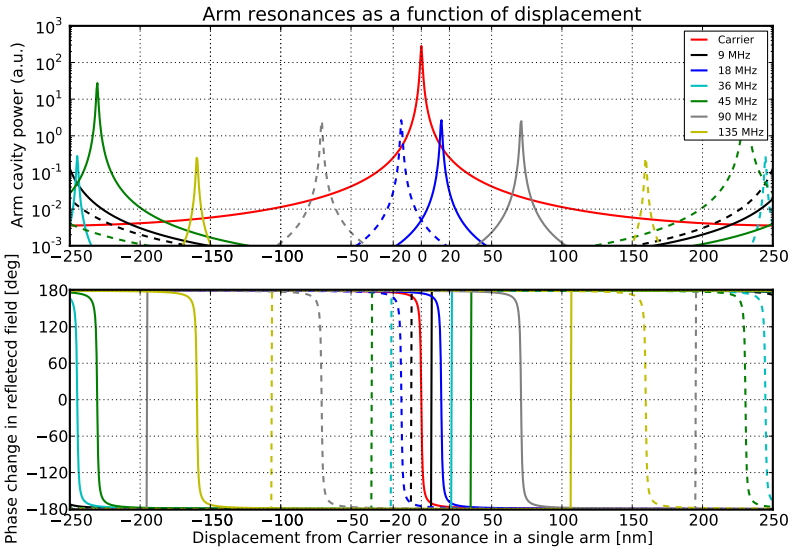

Figure 19: A cartoon plot for shown where each RF sideband can be resonant in a single arm cavity. Note that the line width and amplitudes are not correct.

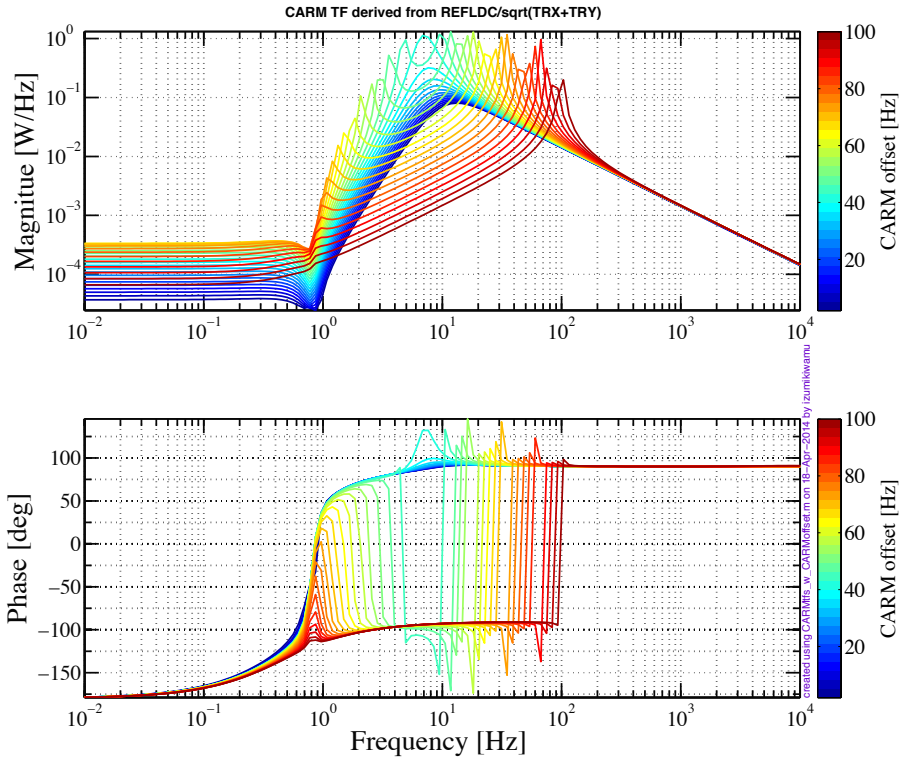

Figure 20: CARM transfer function derived by REFLDC/(TRX + TRY) at various CARM offset points.

References

[1] Available in MIT CVS server

[2] http://www.ligo.caltech.edu/ e2e/

[3] Lisa Barsotti and Matthew Evans, "Lock Acquisition Study for Advanced LIGO" LIGO-T1000294-v1, https://dcc.ligo.org/LIGO-T1000294

[4] Lentickle package for aLIGO full interferometer, available in MIT CVS repository: *export/cvs/iscmodeling/LentickleAligo*

[5] Lisa Barsotti and Peter Fritschel, "Early aLIGO Configurations: example scenarios toward design sensitivity" LIGO-DCC-T1200307 https://dcc.ligo.org/LIGO-T1200307

[6] Koji Arai *et al.* "New signal extraction scheme with harmonic demodulation for power-recycled Fabry-Perot-Michelson interferometers". *Physics Letters A*, 273(1-2):15–24, (2000).

[7] LIGO-T1300688, *ALS Noise Measurements and Model for HIFO-Y*

https://dcc.ligo.org/LIGO-T1300688

[8] R. L. Ward. "Length Sensing and Control of a Prototype Advanced Interferometric Gravitational Wave Detector". PhD thesis, California Institute of Technology, (2010).

[9] Peter Fritschel, " UIM Coil Driver modifications for larger range" LIGO-DCC-T1400223-v1 https://dcc.ligo.org/LIGO-T1400223

[10] Jeff Kissel, DARMmodel_ALS_20140428.m,

sussvn/sus/trunk/QUAD/Common/FilterDesign/HierarchicalControl/

[11] KI, "Status update of aLIGO lock acquisition simulation (20131018)" LIGO-DCC-G1301162 https://dcc.ligo.org/LIGO-G1301162